Supplemental Information

AXL Is a Driver of Stemness in Normal Mammary Gland

and Breast Cancer

Agnete S.T. Engelsen, Katarzyna Wnuk-Lipinska, Sebastien Bougnaud, Fanny A. Pelissier Vatter, Crina Tiron, René Villadsen, Masaru Miyano, Maria L. Lotsberg, Noëlly Madeleine, Pouda Panahandeh, Sushil Dhakal, Tuan Zea Tan, Stacey D'mello Peters, Sturla Grøndal, Sura M. Aziz, Silje Nord, Lars Herfindal, Martha R. Stampfer, Therese Sørlie, Rolf A. Brekken, Oddbjørn Straume, Nils Halberg, Gro Gausdal, Jean Paul Thiery, Lars A. Akslen, Ole W. Petersen, Mark A. LaBarge, and James B. Lorens

Table S1. A unique 70-gene AXL MaSC gene signature

Mu Gene	Dir	Illumina ID	*Hu* Gene
Axl	1	ILMN_2651715	AXL
Supt3h	1	ILMN_1213872	SUPT3H
Elp2	1	ILMN_1216985	ELP2
Fbxo3	1	ILMN_1228298	FBXO3
Anp32a	1	ILMN_1230271	ANP32A
Selp	1	ILMN_1236889	SELP
Tmem154	1	ILMN_1237114	TMEM154
LOC100047935	1	ILMN_1239211	RPL5
Bhlhb9	1	ILMN_1251595	BHLHB9
Artn	1	ILMN_1254114	ARTN
Mrps12	1	ILMN_1254734	MRPS12
Aifm2	1	ILMN_1259418	AIFM2
Tnc	1	ILMN_2463180	TNC
Pbx2	1	ILMN_2599858	PBX2
Rab27a	1	ILMN_2614966	RAB27A
Oas1g	1	ILMN_2628822	OAS1
Ing4	1	ILMN_2639665	ING4
Mrpl3	1	ILMN_2643264	MRPL3
P2ry1	1	ILMN_2684316	P2RY1
Arfgap1	1	ILMN_2700126	ARFGAP1
Fbxo32	1	ILMN_2715893	FBXO32
Ss18l1	1	ILMN_2726159	SS18L1
Cdc42ep3	1	ILMN_2733185	CDC42EP3
Coasy	1	ILMN_2741236	COASY
Chchd10	1	ILMN_2749037	CHCHD10
Asb2	1	ILMN_2765759	ASB2
Pxdn	1	ILMN_2828896	PXDN
Actg2	1	ILMN_2839313	ACTG2
B230339M05Rik	1	ILMN_2894574	RALGAPB
Atp2a3	1	ILMN_2900462	ATP2A3
Acta2	1	ILMN_2923445	ACTA2
Ubac2	1	ILMN_2949605	UBAC2
Ccrl1	1	ILMN_2983624	CCRL1
Trub2	1	ILMN_2983686	TRUB2
Tnrc18	1	ILMN_3003152	TNRC18
Stk4	1	ILMN_3004142	STK4
Dyrk1b	1	ILMN_3053158	DYRK1B
Fam173a	-1	ILMN_1215218	FAM173A
Apoe	-1	ILMN_1216042	APOE
Taf5	-1	ILMN_1218205	TAF5
Pcdh10	-1	ILMN_1228833	PCDH10
1500015O10Rik	-1	ILMN_1249000	C2orf40
Slc19a2	-1	ILMN_1250531	SLC19A2
Mal2	-1	ILMN_1252628	MAL2
Cdk5r1	-1	ILMN_1259339	CDK5R1
Akr1c18	-1	ILMN_1260323	AKR1C3
Tnfrsf12a	-1	ILMN_2424299	TNFRSF12A
Tmem2	-1	ILMN_2430220	TMEM2
Ccar1	-1	ILMN_2516266	CCAR1
Lmna	-1	ILMN_2597710	LMNA
Ell3	-1	ILMN_2627179	ELL3

Mu Gene	Dir	Illumina ID	*Hu* Gene
Hexim1	−1	ILMN_2631994	HEXIM1
Cdkn1a	−1	ILMN_2634083	CDKN1A
P2ry6	−1	ILMN_2663130	P2RY6
Ppp1r3c	−1	ILMN_2667091	PPP1R3C
2200001I15Rik	−1	ILMN_2678637	FAM25A
Hbegf	−1	ILMN_2698449	HBEGF
Nanos1	−1	ILMN_2701355	NANOS1
Rpusd4	−1	ILMN_2718974	RPUSD4
Fnip1	−1	ILMN_2725155	FNIP1
Rrp12	−1	ILMN_2728118	RRP12
Snap29	−1	ILMN_2730767	SNAP29
Tec	−1	ILMN_2752933	TEC
Fosb	−1	ILMN_2778279	FOSB
Wif1	−1	ILMN_2857748	WIF1
Rps2	−1	ILMN_2946616	RPS2
Arhgap20	−1	ILMN_2959729	ARHGAP20
Fhl1	−1	ILMN_3117381	FHL1
Lif	−1	ILMN_3137287	LIF
Sfrs5	−1	ILMN_3148662	SRSF5

Figure S1. Controls for RNA *in situ* experiments
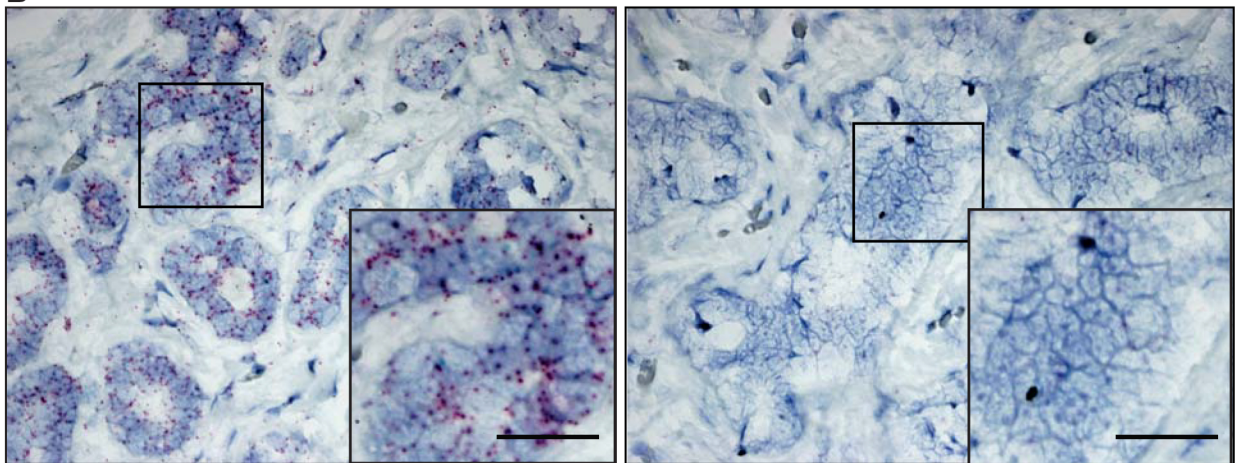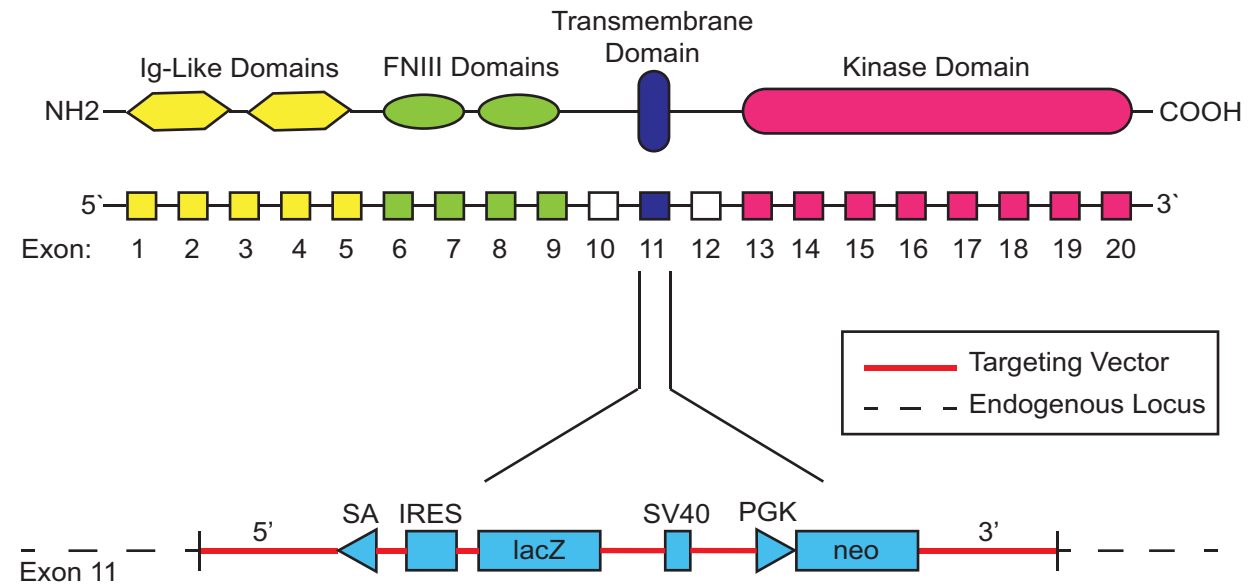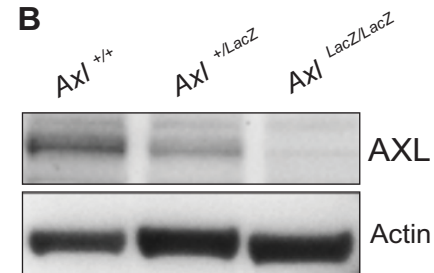
A
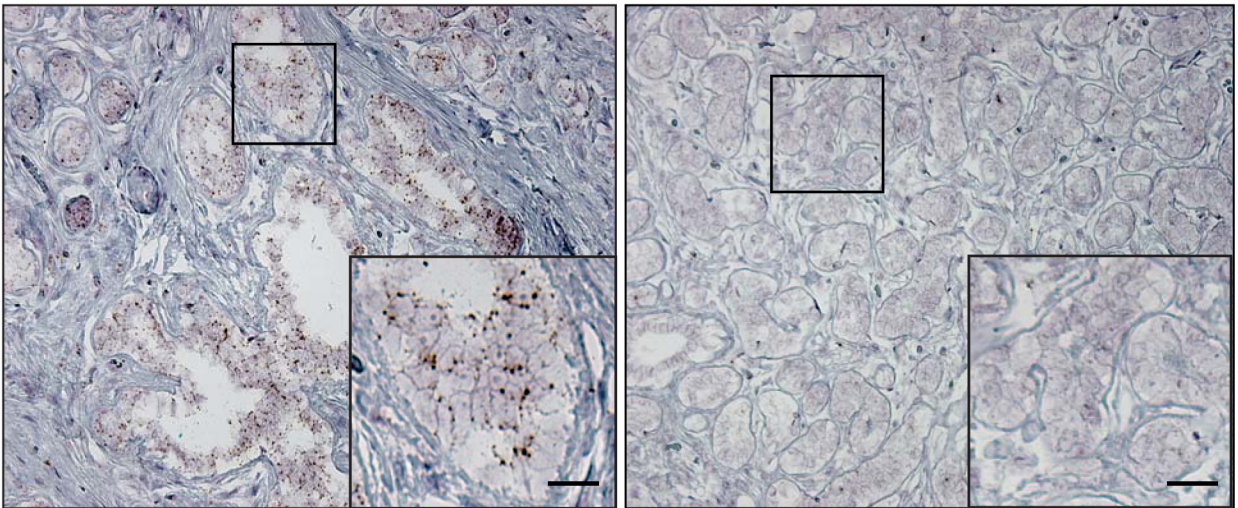
B

Figure S2. Description of the AXL-targeting mutation in B6.129P2-*Axltm1Dgen/J* mice
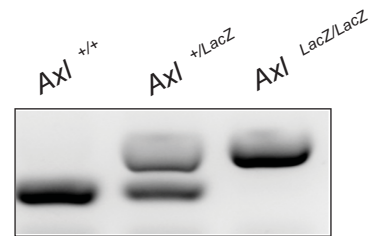
A

B

C

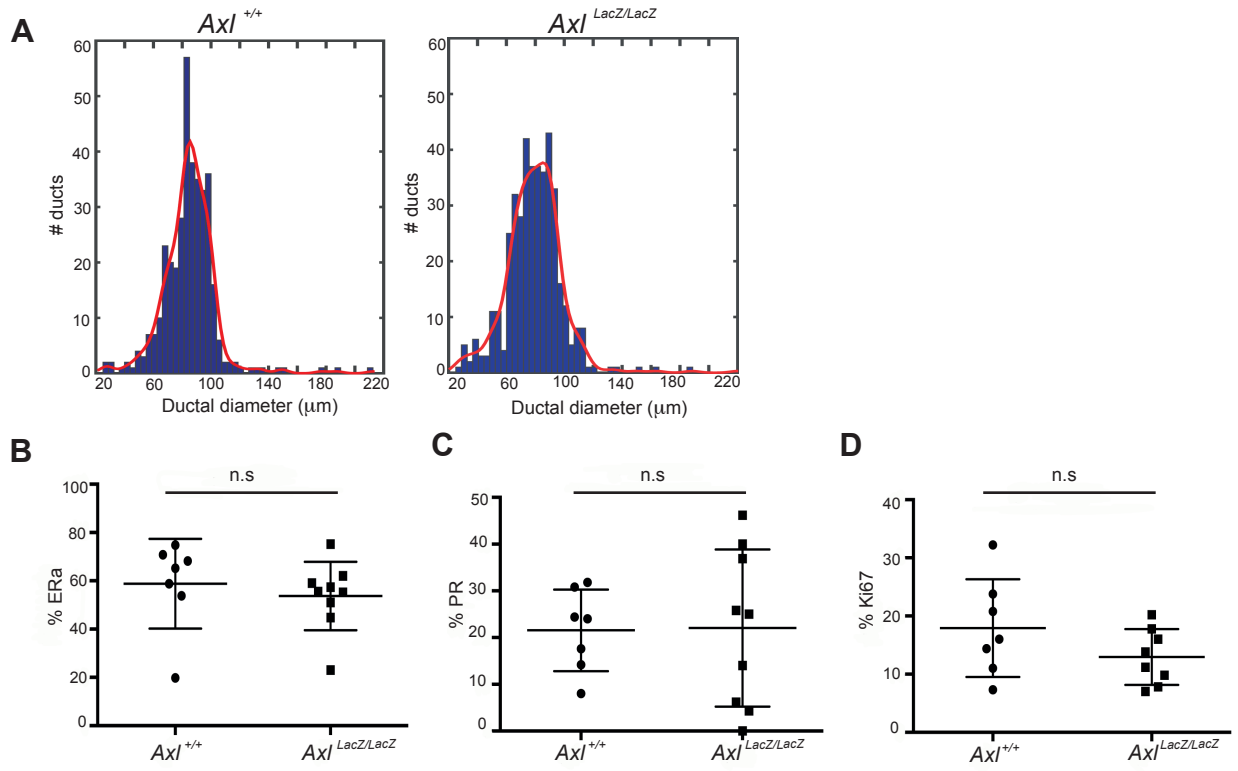# Figure S3. Characterization of AXL null mammary glands

Figure S4. Analysis of mammary gland whole mounts from pubescent warfarin-treated mice

A

B

Treatment

0 1 2 3 4 5 6 7

Weeks after birth

Vehicle-treated

Warfarin-treated

0.5 cm

C

TEB/ gland

* * *
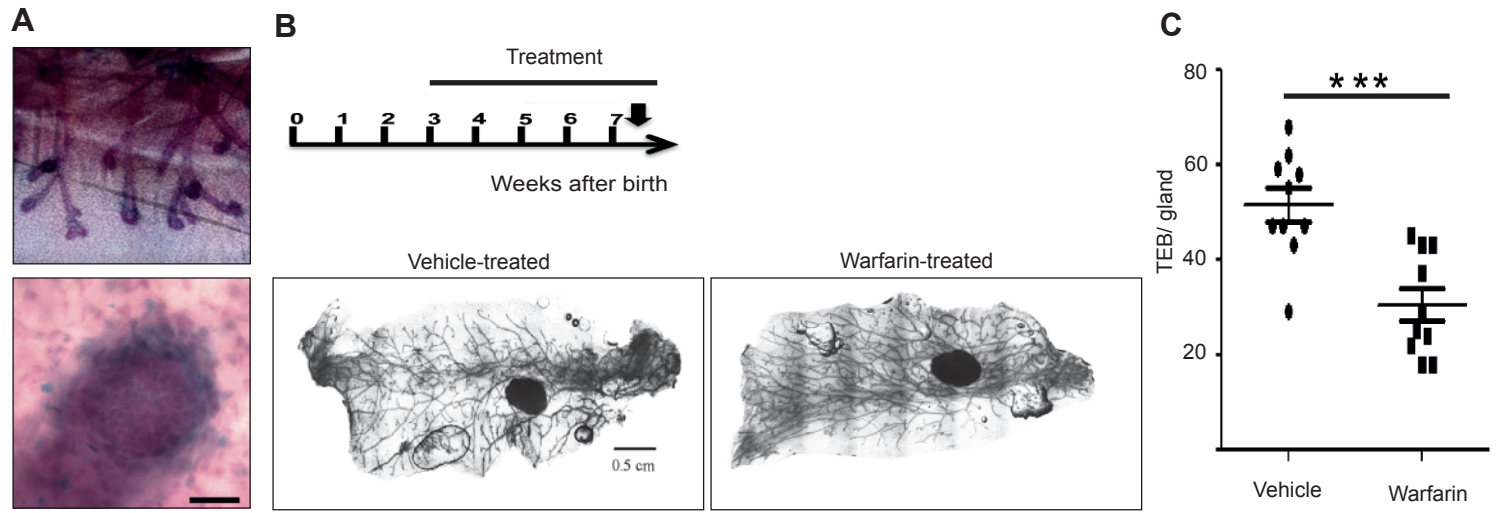
80

60

40

20

Vehicle   Warfarin

Figure S5. The AXL-stem gene expression signature is elevated in basal-like tumors in the Metabric breast cancer patient cohort
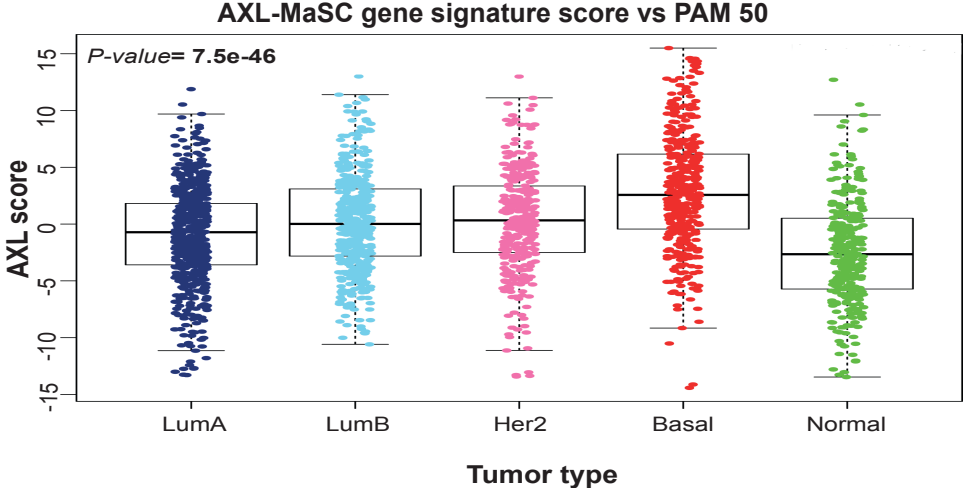
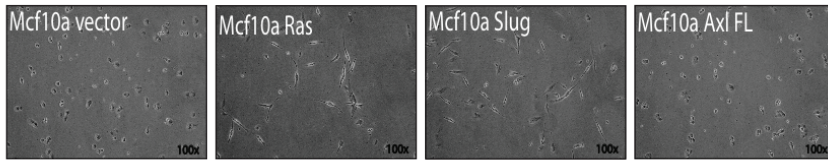# Figure S6. AXL overexpression is not sufficient to induce EMT in MCF10a cells
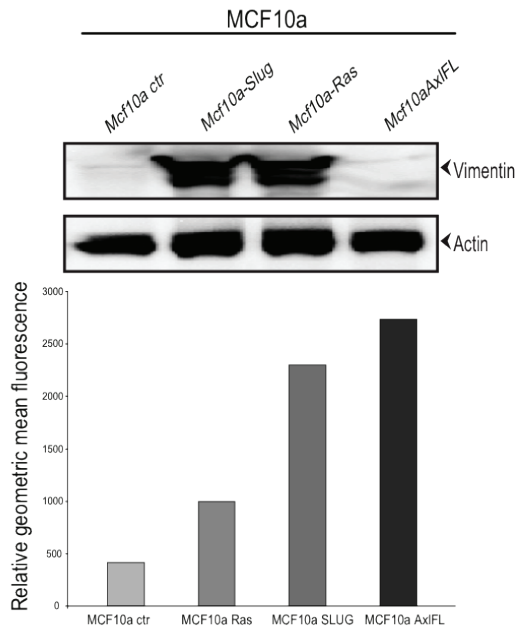
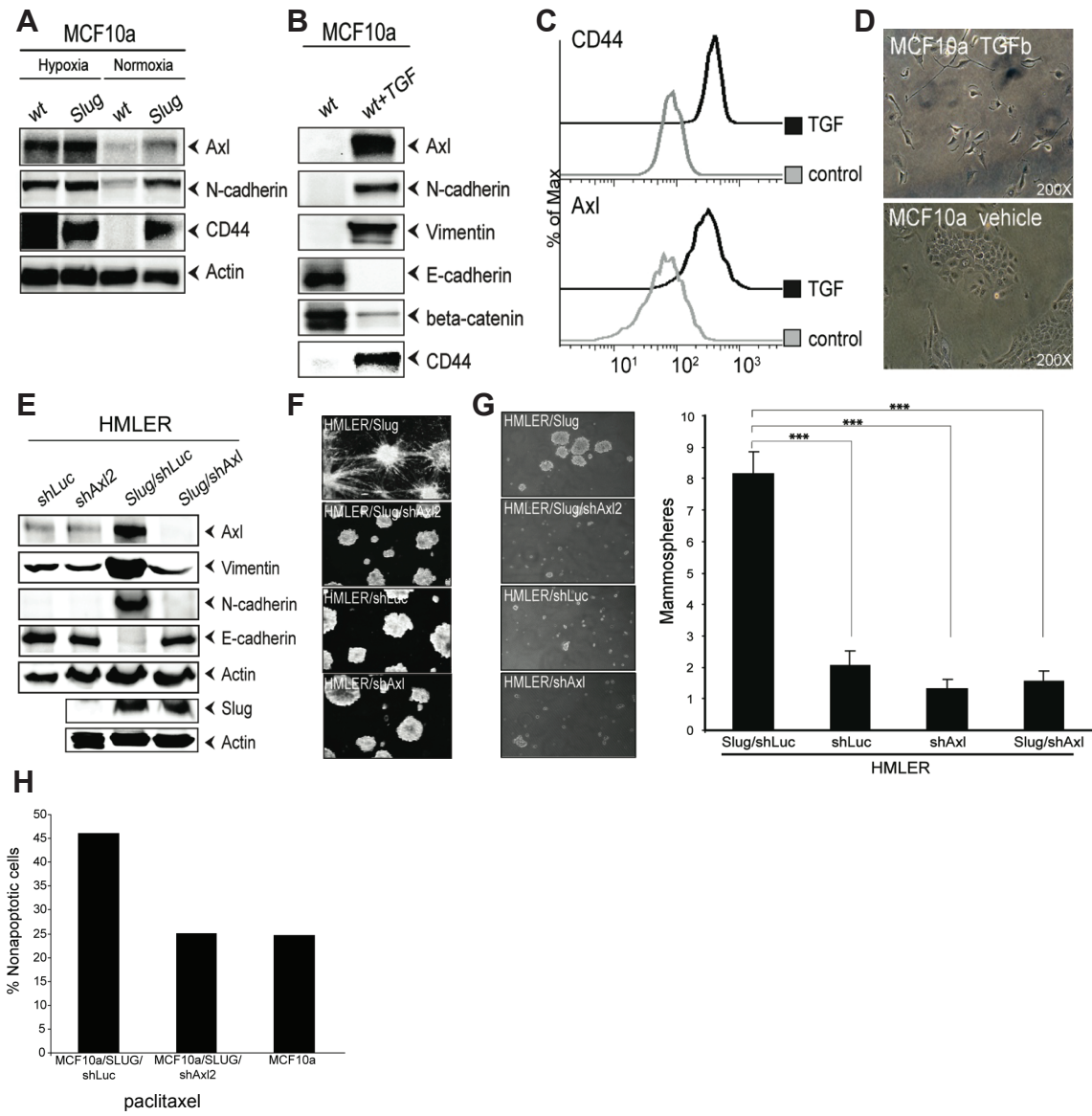# Figure S7. AXL is required for Slug-mediated epithelial plasticity

A MCF10a

	Hypoxia		Normoxia	
	wt	Slug	wt	Slug

◄ Axl
◄ N-cadherin
◄ CD44
◄ Actin

B MCF10a

	wt	wt+TGF

◄ Axl
◄ N-cadherin
◄ Vimentin
◄ E-cadherin
◄ beta-catenin
◄ CD44

C

CD44

TGF
control

Axl

% of Max

TGF
control

10^1 10^2 10^3

D

MCF10a TGFb 200X

MCF10a vehicle 200X

E HMLER

	shLuc	shAxl2	Slug/shLuc	Slug/shAxl

◄ Axl
◄ Vimentin
◄ N-cadherin
◄ E-cadherin
◄ Actin
◄ Slug
◄ Actin

F

HMLER/Slug
HMLER/Slug/shAxl2
HMLER/shLuc
HMLER/shAxl

G

HMLER/Slug
HMLER/Slug/shAxl2
HMLER/shLuc
HMLER/shAxl

Mammospheres

10
9
8
7
6
5
4
3
2
1
0

*** *** ***

Slug/shLuc   shLuc   shAxl   Slug/shAxl

HMLER

H

% Nonapoptotic cells

50
45
40
35
30
25
20
15
10
5
0

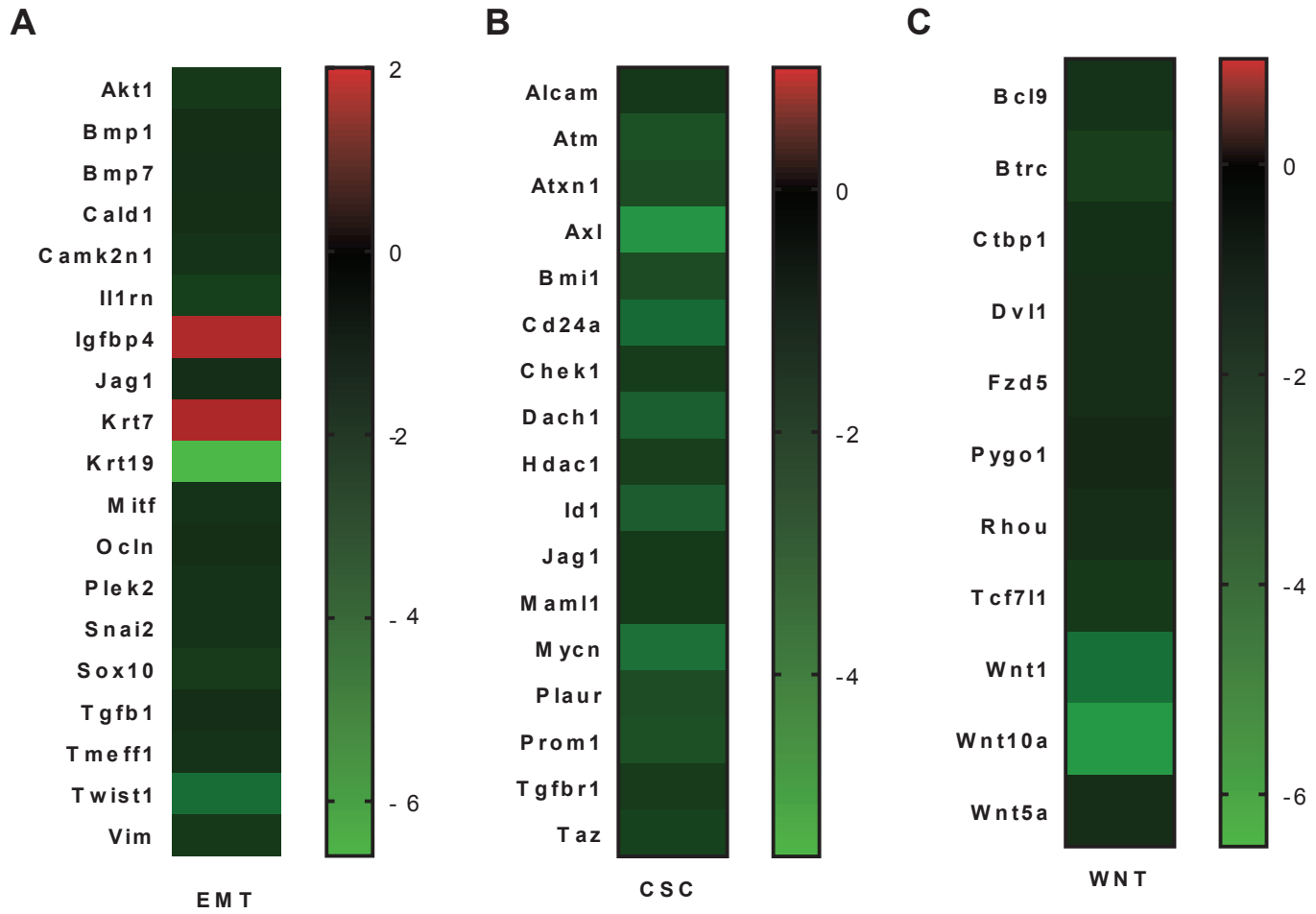MCF10a/SLUG/shLuc   MCF10a/SLUG/shAxl2   MCF10a

paclitaxel

Figure S8. Deregulated signaling pathways of AXL null WNT induced tumors

Supplemental Table and Figure Legends

Table S1. A unique 70-gene AXL MaSC gene signature (related to Figure 5A-B, Figure 6A-C)

The top 70 differentially expressed genes (33 down-regulated and 37 up-regulated by rank product test) determined by Illumina MouseWG-6 v2.0 Expression BeadChip Array gene expression analysis of mRNA isolated from FACS-sorted FDG^{high} $AXL^{+/LacZ}$ and FDG^{high} $AXL^{LacZ/LacZ}$ cell populations. Mu=murine, Hu= human. Dir= direction (1=up, -1=down).

Figure S1. Controls for RNA *in situ* experiment (related to Figure 1 J-N)

(A) Appropriate controls for RNA in situ experiment for single RNA in situ approach with chromogen DAB (brown). Left image shows positive control probe targeting the housekeeping gene PPIB, and right image shows the negative control probe targeting the bacterial DapB gene. Counterstain hematoxylin. (B) Appropriate controls for the dual RNA in situ approach. Left image shows positive control probes targeting the housekeeping gene PPIB (C2: chromogens AP-based Fast Red), as well as POLR2A (C1: chromogen HRP-based green) for the dual approach. Right image show hybridization with negative control probes targeting the bacterial gene DapB, each detection channel (C1 and C2) has its own negative control probe, Counterstain hematoxylin. Scalebar 50 μm.

Figure S2. Description of the AXL-targeting mutation in B6.129P2-*AXL$^{tm1Dgen/J}$* mice (related to mice described in Figure 4. Gene signatures derived from these mice are further described in Table S1, Figure 5 and Figure 6. These mice has been crossed with MMTV-Wnt1 mice as shown in Figure 7I-J)

(A) Schematic illustration of the *LacZ-Neo* cassette insertion site in exon 11 of the murine AXL gene, disrupting AXL protein expression. A 5' splice acceptor ensures that the LacZ open reading frame is spliced into the endogenous AXL mRNA under control of the murine AXL promoter. (B) Western blot analysis of murine AXL expression in dissociated lung tissue from wildtype ($AXL^{+/+}$), heterozygous ($AXL^{+/LacZ}$), and homozygous ($AXL^{LacZ/LacZ}$) mice of the B6.129P2-*AXL^{tm1Dgen}*/J strain (The Jackson Laboratory, Bar Harbour, ME). AXL protein expression from *LacZ*-insertion allele is undetectable. (C) PCR product (http://jaxmice.jax.org/protocolsdb/) from different genotypes of B6.129P2-*AXL^{tm1Dgen}*/J mice (wildtype ($AXL^{+/+}$), heterozygous ($AXL^{+/LacZ}$), and homozygous ($AXL^{LacZ/LacZ}$). Larger sized band represents *LacZ*-insertion allele.

Figure S3. Characterization of AXL null mammary glands (related to Figure 4 A-C)

(A) Mammary gland whole-mounts from adult (16 week-old) $AXL^{+/+}$ (wildtype) and $AXL^{LacZ/LacZ}$ (*AXL*-null) mice were harvested and processed for characterization by carmine alum staining. Ductal diameters were quantified with MATLAB using image segmentation analysis of the carmine-alum stained glands. The Kolmogorov–Smirnov test rejected the hypothesis that ductal diameters of wildtype $AXL^{+/+}$ and $AXL^{LacZ/LacZ}$ are derived from the same distribution (p= 9.23x10-7). (B-D) Histopathologic quantification of (B) ERα, (p= 0.35), (C) PR (p= 0.96) and (D) Ki67, (p= 0.24) immunohistochemistry of mammary duct FFPE tissue sections of adult AXL+/+ (wildtype) $AXL^{LacZ/LacZ}$ mammary glands. n.s= non-significant by Mann-Whitney, non-parametric test.

Figure S4. Analysis of mammary gland whole mounts from pubescent warfarin-treated mice (related to Figure 5E)

(A) β-galactosidase activity is shown in terminal end buds (TEB) of mammary gland whole-mounts of 6-week old prepubescent $AXL^{+/LacZ}$ mice stained by β-galactosidase histochemistry and counterstain by carmine alum. β-galactosidase activity was prominent in cells located to the cap region of TEBs. Scalebar: 100μm. (B) Schematic overview of warfarin treatment regimen. Peroral warfarin administration were initiated at in 3 week-old mice post-weaning. Representative composite images of carmine alum stained mammary gland whole-mounts from mice treated for 5 weeks with either pure or warfarin (1 mg/L) containing drinking water. (C) Quantification of terminal end buds (TEB) in carmine alum stained mammary gland whole mounts harvested from 8 week-old control and warfarin treated animals (t-test, p=0.0004). Duration of treatment: 5 weeks.

Figure S5. The AXL-stem gene expression signature is elevated in basal-like tumors in the Metabric breast cancer patient cohort (related to Figure 6C)
The Metabric breast cancer patient cohort (n=1,980) (Curtis et al., 2012) was interrogated with the AXL MaSC gene expression signature (AXL-stem, Table S1) to assess the influence of the novel AXL stem gene expression signature on clinical endpoints. The AXL-stem score correlated with tumor subtype of PAM50 subtyped tumors is shown; the AXL score is significantly elevated in the basal-like tumors (P = 7.5×10^{-46}, Kruskal-Wallis rank test).

Figure S6. AXL overexpression is not sufficient to induce EMT in MCF10a cells (related to Figure 7 A-D)
MCF10a cells transduced with control vector or retroviral expression vector encoding AXL, Slug or Ha-Ras(G12V) as well as GFP reporter-gene. Post transduction, cells were FACS sorted based on their GFP expression, and protein expression of Vimentin were measured by Western blotting (upper). Cell-surface expression of AXL were quantified by flow cytometry (middle) (>100,000 events) and displayed as geometric mean. Phase contrast images displaying cell morphologies of control and AXL-, Slug- and Ha-Ras(G12V)-expressing MCF10a cells are shown below.

Figure S7. AXL is required for Slug-mediated epithelial plasticity (related to Figure 7 A-F)
(A) AXL is induced by hypoxia. Western blot analysis of CD44, N-cadherin (CDH2), and AXL protein expression in MCF10a/control and MCF10a/Slug cells grown under normoxic and hypoxic (1% O2) conditions. (B) AXL is induced by TGFb. Western blot analysis of AXL, CD44, epithelial (E-cadherin, ß-catenin) and mesenchymal (vimentin, N-cadherin) marker expression. (C) Flow cytometric analysis of CD44 and AXL surface levels; and (D) Phase contrast images of MCF10a cell morphology, after culture with TGFb (10 ng/ml) or vehicle for 7 days. (E) AXL is required for Slug-mediated mesenchymal and stem cell traits in HMLER cells. HMLER transduced with control or Slug retroviral expression vectors (with GFP reporter gene), as well as AXL-targeting shRNA (shAXL2) or control luciferase shRNA (shLuc) vectors (with RFP reporter gene), were sorted for GFP and RFP, and analyzed for by western blot for expression of AXL, Slug (SNAI2), epithelial (E-cadherin, β-catenin) and mesenchymal (vimentin, N-cadherin). β-actin was used as a loading control. (F) AXL is required for EMT-induced stellate colony formation. Phase contrast images of HMLER/shLuc, HMLER/shAXL2 and HMLER/Slug/shAXL2 and HMLER/Slug/shLuc cell colonies in 3D embedded lrECM (matrigel). (G) AXL is necessary for EMT-induced mammosphere formation. Quantification of mammosphere formed by HMLER/shLuc, HMLER/shAXL2 and HMLER/Slug/shAXL2 and HMLER/Slug/shLuc cells. Y-axis represents total number of mammospheres formed per well (mean ±S.D., n= 6; *** p<0.0001, t-test). (H) AXL signaling is required for EMT-induced drug resistance. Multicolor flow cytometry analysis of MCF10a cells transduced with control or Slug retroviral vector following 24 hour treatment with paciltaxel (30 μg/ml). The percentage of non-apoptotic cells represents the % viable cells post-treatment (of >100,000 total events) within the AnnexinV negative, Sytox Blue negative gate for each cell line.

Figure S8. Deregulated signaling pathways of AXL null WNT induced tumors (related to Figure 7 I-K)
Pathway focused RT2 Profiler TM PCR arrays demonstrate alterations in (A) EMT signaling pathway, (B) CSC pathway and (C) WNT pathway analysed in 6 Axl^{+/+} wild-type and 4 $AXL^{LacZ/LacZ}$ (Axl-null) Wnt1- induced tumors. The gene expression levels of the Axl-null (n=4) samples were quantified relative to the expression levels for WT samples (n=6) after normalization to the levels of the suitable housekeeping genes (ACTB, B2M, GAPDH, GUSB, HSP90AB1) in the panel. Data in heatmaps are reported as mean fold changes.

Transparent Methods

Reagents

Anti-hAXL MAB10C9 (Lorens laboratory), MAB154, AF154 (R&D Systems), Anti-mAXL (sc-1097, Santa Cruz), mouse anti-human Slug (L40Cb, Cell Signaling), rabbit anti-human E-cadherin (24E10, Cell Signaling), rabbit anti-human N-cadherin (ab18203, Abcam), α-actin (A5060, Sigma), mouse anti-human β-catenin (L54E2, Cell Signaling), rabbit anti-human β-catenin (Cell Signaling), mouse rat anti-human Vimentin (MAB2105, R&D Systems), anti-CD227-FITC (Becton Dickinson, clone HMPV), anti-CD10-PE (BioLegend, clone HI10a), anti-CD117- Alexa647 (BioLegend, clone 104D2), EPCAM-BV421 (BioLegend, clone 9C4), anti-CD49f-PE (Chemicon, clone CBL-458P), anti-K14 (Covance, polyclonal rabbit), anti-K19 (Developmental Studies Hybridoma Bank, clones Troma-II and Troma-III), anti-CD44 (Cell Signaling, 3570), anti-CD31-PE (17-0311), anti-CD45-PE (17-0451), and anti-CD11b (11-0112; eBioscience). Imatinib (LC laboratories I-5508) and bemcentinib (also known as BGB324 and R428, BerGenBio AS) (Holland et al., 2010) were prepared in DMSO.

Immunohistochemistry (IHC-P, IHC-F)

IHC-P, fluorescent detection: Paraffin-embedded normal human breast tissue sections (generously provided by Dr. A. Borowsky) were prepared for immunofluorescence and stained as previously described (Garbe et al., 2012) using anti-K14 (Covance, polyclonal rabbit), anti-K19 (Developmental Studies Hybridoma Bank, clone Troma-III), anti-CD117 (BioLegend, clone 104D2), anti-hAXL MAB10C9 (BerGenBio ASA) overnight at 4oC, visualized with fluorescent secondary antibodies (Invitrogen) and 4,6-diamidino-2-phenylindole (DAPI) nuclear stain at room temperature for 1 hour, and imaged using a 710LSM microscope (Carl Zeiss).

IHC-P, chromogenic detection: Paraffin-embedded normal human breast tissue sections were prepared for staining as described (Garbe et al., 2012). Anti-Axl antibody were incubated o/n at 1:6000 dilution (clone EPR19880, Abcam). Peroxidase stain was performed by Ultravision ONE Destection System (Thermo Scientific). Sections were counterstained with hematoxylin and mounted with Entellan (Merck) prior to imaging.

IHC-F: Mammary tissue specimens were embedded in OCT and snap frozen in liquid nitrogen. Cryosections (6μm thickness) were stained with anti-Axl antibody (clone EPR19880, 1:100, Abcam); anti-K14 (clone LL002, 1:100, Monosan); anti-K19 (clone A53-B/A2, 1:100, BioLegend). Alexa Fluor conjugated secondary antibodies (1:500, Invitrogen) and 4,6-diamidino-2-phenylindole (DAPI) nuclear stain.

RNA *in situ* hybridization

In situ detection of *AXL* and *GAS6* mRNA in human mammary FFPE tissue were performed using the RNA Scope technology. Probes and reagents were provided by Advanced Cell Diagnostics (ACD, Hayward, CA). Briefly, human archival mammary gland tissue sections of 5 um thickness were deparaffinized in xylene, followed by dehydration in ethanol. Tissue sections were then incubated in citrate buffer (10 nM/ L, pH 6) maintained at boiling temperature (100oC to 103°C) using a hot plate for 15 minutes, rinsed in deionized water, and immediately treated with 10 μg/ mL protease (Sigma-Aldrich, St. Louis, MO) at 40oC for 30 minutes in a HybEZ hybridization oven (Advanced Cell Diagnostics, Hayward, CA). Hybridization with target probes, preamplifier, amplifier, label probe and chromogenic detection were performed according to ACD's recommendations. Sections were counterstained with hematoxylin and mounted with EcoMount prior to imaging. Assays using archival FFPE specimens were performed in parallel with positive and negative control probes, to ensure interpretable results (Supplementary Figure 4). Histo score analysis were performed to evaluate the heterogeneity in marker expression. Cells were scored and grouped in 5 bins based on the number of dots/ cell (Bin 0= 0 dots/cell, Bin 1= 1-3 dots/ cell, Bin 2= 4-9 dots/ cell, Bin 3= 10-15 dots/cell (<10% dots in clusters), Bin 4= >15 dots/cell (>10% dots in clusters). Each sample was manually scored, and the percentage of cells in each bin recorded. Histo score was calculated by totaling the percentage of cells in each bin according to the given formula. Histo score= 0*(% of cells in bin 0) +1*(% of cells in bin 1) +2*(%of cells in bin 2) +3*(% of cells in bin 3) +4*(% of cells in bin 4). Histo score is provided on the range 0-400.

Human mammary epithelial cells (HMEC) isolation and culture

Pre-stasis human mammary epithelial cells (HMEC) were derived from reduction mammoplasties (n=60) were established and maintained as described (Labarge et al., 2013) in low-stress M87A medium with oxytocin and cholera toxin (Garbe et al., 2012). HMEC of 4th passage or lower were used.

Flow cytometry and FACS sorting

Flow cytometry analysis of MCF10a cells was conducted as described (Gjerdrum et al., 2010). For flow analysis of isolated human breast epithelial organoids and pre-stasis HMEC, cells were recovered following trypsin treatment and resuspended in their media. For enrichment or identification of luminal epithelial and myoepithelial lineages, anti-CD227-FITC (Becton Dickinson, clone HMPV, 1:50) or anti-CD10-PE, -PE-Cy5 or -APC (BioLegend, clone HI10a, 1:50), were used, respectively. Other analysis was carried out with EPCAM-BV421 (BioLegend, clone 9C4), anti-CD49f-PE (Chemicon, clone CBL-458P, 1:50), anti-CD117-Alexa647 (BioLegend, clone 104D2, 1:200) and anti-hAXL MAB10C9 conjugated to Alexa-647 (1:200). MABs were added to the media at 1:50 for 25 minutes on ice, washed in PBS, and sorted or analyzed. KIT-expressing HMEC progenitors were isolated by staining with anti-CD117-PE (BioLegend, clone 104D2, 1:200) and were added to cells in media for 25 min on ice, washed in PBS and sorted on a FACS Vantage SE DIVA (Becton Dickinson). β-galactosidase flow cytometry was done using FluoReporter® lacZ Flow Cytometry Kit (Molecular Probes F-1930). For transplantation assays and organoid assays of murine cells the following sorting strategy were used: freshly dissociated and labeled cells were discriminated from the debris and gated in the forward scatter (FSC-A) and side scatter (SSC-A) plots. Subsequently, the forward scatter Width (FSC-W) versus FSC-A plots were used for doublet cell exclusion. Propidium iodide (PI) staining was used for dead cell discrimination and the APC channel was used as a dump channel for the APC conjugated lineage markers used. Thus, only single, viable, PI-negative, and APC-negative cells were included in the final sort of FDG-high and FDG-low cells used for subsequent experiments. A post-sort analysis was performed to verify purity of the sorted cells and sort numbers were obtained from each sort, however, the cell counts used for subsequent experiments were determined by visualizing and enumerating live healthy single cells. T Data analysis was carried out on 500 000 events using the FlowJo software (Tree Star, Inc., Ashland, OR, USA). SPADE analysis was performed with Cytoscape (www.cytoscape.org) and R (Foundation for Statistical Computing).

High-dimensional Mass cytometry

Mass cytometry analysis of dissociated primary human breast epithelia was described in great detail in (Pelissier Vatter et al., 2018). Primary HMEC strains were generated and maintained as described (Labarge et al., 2013). All tissues were obtained with proper oversight from the Lawrence Berkeley National Laboratory institutional review board. Breast tissue from reduction mammoplasty was manually dissected to enrich for gland-containing material. Stromal tissue was separated from epithelial fragments using a brief treatment with collagenase. The uncultured breast epithelia samples were dissociated as single cells with trypsin. Cells were incubated with cisplatin (WR International, Cat# 89150- 634, 25 mM) for 1 min to assess cell viability (Fienberg et al., 2012), fixed in 1.6% PFA for 10 min at RT, and washed once with Cell Staining Media (CSM, PBS with 0.5% BSA and 0.02% NaN3 with 0.03% saponin). The cells were then resuspended in PBS, and DMSO stocks of the barcoding reagent were added as described (Bodenmiller et al., 2012, Zivanovic et al., 2014). The cells were incubated at RT for 30 min, washed three times with CSM, and then pooled into a single FACS tube for staining with metal-labeled antibodies for 1 hr at RT. After antibody staining, the cells were washed twice with CSM and once with PBS, and then incubated for 20 min at RT or overnight at 4°C with an iridium-containing intercalator (DVS Sciences) in PBS with 1.6% PFA. The cells were then washed three times with CSM and once with PBS, diluted with water to ~106 cells/mL, and filtered through a 40-mm membrane just before analysis by mass cytometry. The scale used before analysis is the arcsinh with the cofactor of 5 ($x\_transf = asinh(x/5)$). After gating out viable and iridium-labeled events, the data were analyzed by applying tSNE. This non-linear dimensionally reduction technique is implemented via Barnes-Hut approximations in the MATLAB toolbox cyt (Amir el at al., 2013). We used the default parameters (initial dimensions, 110; perplexity, 30; and theta, 0.5). The

unsupervised PhenoGraph algorithm in cyt has been used to group cells that are phenotypically similar and cluster these subpopulations using modularity optimization (Levine et al., 2015). tSNE and PhenoGraph were performed only on surface markers. A number of neighbors of 800 was selected. The heatmap was obtained with MATLAB. The accession number for the CyTOF data reported in this paper is Mendeley Data: https://doi.org/10.17632/j7mrbgt3hh.1.

3D-embedded laminin-rich ECM assay
MCF10a or KIT-enriched HMEC were resuspended in media (50000 cells/ µL) and 200 µL of matrigel (BD Sciences 356234) were added to the cells and transferred to a 24-well plate pre-coated with 50 µL of Matrigel, then cultured for 10-12 days prior to microscopy analysis. For immunofluorescence analysis of HMEC colonies, Matrigel smears were fixed in methanol/acetone 1:1 at -20°C for 20 min, incubated with blocking buffer overnight at 4°C, incubated with anti-K14 and anti-K19 overnight at 4°C, extensively washed with PBS, then incubated with fluorescent secondary antibodies overnight at 4°C, and washed overnight at 4°C before mounting coverslips with Fluormount G. Insert Keratin 5 (murine).

Mammosphere formation assay
Mammosphere culture of MCF10a was performed as previously described(Dontu et al., 2003). Single cells were plated in ultra-low attachment plates (Corning, Acton, MA, USA) 20,000 viable cells/ ml. For mammosphere assays of HMEC, flow cytometry sorted KIT+ enriched HMEC (p4) were resuspended in mammosphere media (MammoCult human medium kit (StemCell 05620, enriched with heparin and hydrocortisone) at 25,000 cells/ mL in polyHema (0.133 mL at 12 mg/ ml in 95% EtOH) treated 24-well plates (in triplicate) and cultured for 10 days. Large (≥70 µm) and hollow mammospheres were identified by microscopy of each well. Total mammospheres per well were quantified using ImageJ. Secondary mammospheres were prepared by trypsinizing and resuspending for cell from first passage mammospheres. For the immunofluorescence, mammospheres were fixed in 4% paraformaldehyde for 5 min, blocked with PBS, 5% normal goat serum, 0.1% Triton X-100, and incubated with anti-K14 (1:1000, Covance, polyclonal) and anti-K19 (1:10, Developmental Studies Hybridoma Bank, clone Troma-III) overnight at 4°C, then visualized with fluorescent secondary antibodies (Invitrogen) incubated with sections for 2 hours at room temperature.

Gene expression analysis
Global gene expression analysis of HMEC lineage was performed on FACS sorted (FACS Vantage SE DIVA, Becton Dickinson) pre-stasis HMEC strains 240L and 122L cells (4th passage). Total RNA from FACS-enriched primary culture cells was isolated with TRIzol (Invitrogen) and RNeasy Mini column (Qiagen) and evaluated using Bioanalyzer (Agilent Technologies). Gene expression levels were measured using the Illumina HumanHT-12 v4 Expression BeadChip whole-genome expression array. The Illumina Bead Array data were quality controlled in Genome Studio and both probe level and gene level data were imported into J-Express Pro (http://jexpress.bioinfo.no) for analysis. After quantile normalization both datasets were log2 transformed. Correspondence Analysis (Fellenberg et al., 2001) was performed on the datasets, together with Hierarchical Clustering of the samples using a Pearson correlation measure on a per gene mean centered version of the data.

Gene expression analysis of FDG FACS-sorted 16 week old nulliparous $AXL^{+/LacZ}$ and $AXL^{LacZ/LacZ}$ (B6.129P2-$AXL^{tm1Dgen}$ strain, Jackson Labs) was conducted using the Illumina MouseWG-6 v2.0 Expression BeadChip (BD-201-0202, BD-201-0602). Log2 quantile normalized of the gene expression data were used for unsupervised hierarchical clustering, gene signature analysis and differentially expressed genes. Hierarchical clustering was performed using Pearson's correlation as distance measurement. Gene signatures among cell population were determined by comparing the gene expression levels and available molecular signatures of the mammary cell subpopulations (Lim et al., 2009) using GSEA software package (Subramanian et al., 2005). Differentially expressed genes between $AXL^{+/LacZ}$ FDG^{high} and $AXL^{LacZ/LacZ}$ FDG^{high} cell groups were identified using Rank Product method. The genes with a p-value <0.01 and fold change >= 1.5 were considered as differentially expressed genes. All analyses were performed using R version 3.2.2. To assess the influence of AXL and its downstream targets on survival of breast cancer patients, we

derived a score capturing the expression of these genes. The score is the sum of the top 70 genes from the rank product test, of which 33 genes were downregulated and 37 upregulated, adjusted for expected directionality. For genes represented by multiple probes, mean signal intensity was used. The influence on breast cancer-specific survival and putative difference between molecular subtypes were investigated in the Metabric cohort, composed of 1980 breast cancer patients enrolled at five different hospitals in the UK and Canada (Curtis et al., 2012). Gene expression was assessed using the Illumina HT-12 v3 microarray and normalized data was downloaded from the European Genome-phenome Archive (EGA) data portal. Missing values were imputed using the impute.knn function as implemented in the R library 'impute' with default settings (R package version 1.46.0.). The data was batch adjusted for hospital effect using the pamr.batchadjust function in the 'pamr' library with default settings. Association between the score and molecular subtypes was tested using Kruskal-Wallis rank test, and correlations were estimated with Spearman's rank correlation. Survival analyses were performed using Cox proportional hazards regression model as implemented in the R library 'rms'. The generic EMT 315 gene expression signature were used to compute the EMT score of the FDG high $Axl^{+/LacZ}$ and $Axl^{LacZ/LacZ}$ populations as previously described (Tan et al., 2014).

MMTV-Wnt1 mammary tumor cells (6 from *MMTV-Wnt1:Axl*$^{+/+}$ and 4 from *MMTV-Wnt1:Axl*$^{+/LacZ}$) were analyzed using RT2 Profiler TM PCR arrays (96 X 4) (Mouse WNT signaling pathway PAMM-043ZG-4; Mouse Epithelial to Mesenchymal Transition PAMM-090ZG-4 ; Mouse Cancer Stem cells PAMM-176ZG-4, Qiagen) as per the manufacturer's guidelines. The tumors were harvested from mice and flash frozen for RNA isolation. Total RNA extraction was performed using RNeasy Mini Kit (Qiagen), and cDNA was synthesized for RT-qPCR using the RT2 first strand kit (Qiagen) as recommended by the manufacturer. RT-qPCR was performed on a LightCycler® 480 (Roche) using RT² SYBR Green qPCR Mastermix (Qiagen) for SYBR Green detection of each reaction and expression levels were determined using the ΔΔCt method. Expression levels were normalized to housekeeping genes (ACTB, B2M, GAPDH, GUSB, HSP90AB1) with small changes in their expression across different sample groups (differences in CT values less than 1). The p values were calculated based on a Student's t-test (unpaired; *P<0.05, **P<0.01, ***P<0.001) from the 2-ΔΔCT values obtained for each gene in the WT group and KO groups.

Retroviral vectors
MCF10a (American Type Culture Collection, Rockville, MD) were cultured as described (Gjerdrum et al., 2010). The CRU5-IRES-hSlug retroviral vector prepared as described (Gjerdrum et al., 2010). Retroviral production and infections were conducted using Phoenix A retroviral packaging cells as described (Swift et al., 2001).

Immunoblotting
MCF10A cells were lysed using NP40 Cell Lysis Buffer (40 mM HepesNAOH, 75 mM NaCl, 2 mM EDTA, 1% NP40, phosphatase inhibitor cocktail tablet, protease inhibitor cocktail tablet (Roche)). Running of SDS/PAGE gel and immunoblotting were carried out according to standard procedures.

Animal studies
Animal experiments were approved by the Institutional Animal Care Research Authority and in accordance with The European Convention for the Protection of Vertebrates Used for Scientific Purposes. Animals were housed in a germ-free environment in filter top cages. Environmental parameters were monitored by the Laboratory Animal Facility of UIB and followed the institutional SOP. Animals were provided certified laboratory feed and sterile drinking water ad libitum. Clinical observation of animal appearance were recorded daily. At study termination the animals were anesthetized by Sevoflurane and euthanized by cervical dislocation euthanized following Institutional SOP.

Mammary transplantation assay
Mammary glands were dissected from adult (12-16 week old) B6.129P2-*AXL*^{tm1Dgen} heterozygous and homozygous mice (Jackson Labs), washed in cold PBS, minced and incubated overnight at 37˚C in dissociation medium containing EpiCult-B Basal Mouse Medium (05611, STEMCELL Technologies) supplemented with 5% fetal bovine serum and

1.7 mg/ ml collagenase XI (C9697, Sigma). After dissociation and centrifugation, cells were suspended in a 1: 4 mixture of cold Hanks Balanced Salt Solution Modified (37250, STEMCELL Technologies) supplemented with 2% FBS and ammonium chloride (07850, STEMCELL Technologies) in order to lyse red blood cells. Dissociation was ended by proteolysis using pre-warmed 0.25% trypsin-EDTA followed by incubation in pre-warmed 5 mg/mL dispase with 0.1 mg/mL DNase I solution (07900, STEMCELL Technologies). FluoReporter® LacZ Flow Cytometry Kit (F-1930, Molecular Probes) was used for fluorescent β-galactosidase detection followed by FACS. Protocol provided by manufacturer was followed, with minor modifications. Briefly, isolated mammary epithelial cells were suspended in staining medium containing Hanks Balanced Salt Solution Modified (37250, STEMCELL Technologies) supplemented with 2% FBS and 300 µM chloroquine to inhibit lysosomal β-galactosidase activity. The same volumes of 2 mM FDG working solution and cell suspension were pre-warmed at 37˚C for 10 or 20 minutes, respectively. Cell suspension was loaded with FDG working solution, mixed and incubated at 37˚C for exactly one minute. The reaction was stopped by adding ice cold staining medium. Cells were analyzed and sorted immediately by FACS ARIA (Becton Dickinson) cell sorter. Gates were set following intensity of fluorescein signal and there were selected distinct positive and negative populations.

Recipient 4 week old athymic Nude-*Foxn1^{nu}* mice (Harlan Laboratories) were prepared by clearing the epithelium of the inguinal mammary glands on both sides to avoid interference from the host`s gland. Distinct fluorescein positive cells in limiting dilution series (10 000, 1000, 100) were implanted in 25 µl of BD Matrigel (BD Biosciences) on the one side and limiting serial dilution (10 000, 1000, 100) of distinct fluorescein negative cells on the other side as a control. The wound was closed using fine sutures. After 8 weeks restored mammary glands were dissected, spread on the glass slide and submerged in 2% paraformaldehyde in PBS for 3 hours. The mammary glands were then rehydrated in a series of ethanol dilutions (70%, 50%, 25%) and distilled water. Rehydrated glands were stained overnight in Carmine alum solution containing 1 g Carmine (C1022, Sigma), 2.5 g aluminium potassium sulphate (A7210, Sigma) per 500 ml of distilled water. Next, glands were dehydrated in a series of ethanol dilutions (70%, 95%, 100%) and bleached in xylenes for 48 hours. At the end mounted with Organo/Limonene Mount (O8015, Sigma). Samples were let dry overnight before imaging by light microscopy. Repopulating frequency and confidence intervals were calculated using limiting dilution analysis using Extreme Limiting Dilution Analysis (ELDA) software (http://bioinf.wehi.edu.au/software/elda/; (Hu and Smyth, 2009). ELDA uses a general linear model approach to calculate a maximum likelihood estimate from which the stem cell frequency is derived. Pairwise tests for differences in stem cell frequencies are determined by likelihood ratio tests using the asymptotic chi-square approximation to the log-ratio.

Mammary gland phenotype studies
Heterozygous and homozygous mice of B6.129P2-*AXL^{tm1Dgen}* strain (Jackson Labs) were sacrificed at 16 weeks, and mammary gland tissue harvested for Carmine alum whole-mount staining. Separate glands where harvested for formalin fixation and parafin embedded for subsequent H&E staining, immunofluorescence and IHC-P as described. Paraffin-embedded tissue sections from B6.129P2-*AXL^{tm1Dgen}* reporter mice were de-parafinized, antigen-retrieved (citrate buffer), and incubated 45 minutes in blocking buffer (5% goat serum in PBS w. 0.1% Triton X-100). Sections were then stained with primary antibodies chicken anti-beta galactosidase (1:100, ab9361, abcam), rat anti-Cytokeratin 8 (1:100, clone TROMA-1), and rabbit anti-Keratin 5 (1:400, PRB-160P-100, BioLegend) overnight at 4°C. To avoid cross-reactivity between the secondary antibodies, the samples were first incubated 45 minutes with AF647 goat anti-rabbit (1:200, A21244, Invitrogen) together with AF546 goat anti-rat (1:200, A11081, Invitrogen), then washed 3 times with PBS-T before a second round of 45 minutes incubation with AF488 rabbit anti-chicken IgY (IgG) Fc fragment specific (1:200, Jackson ImmunoResearch). Samples were then washed and mounted with ProLong Diamond Antifade Mountant with DAPI nuclear stain (P36962, Molecular Probes/Invitrogen) and imaged the next day with a Leica TCS Sp8 confocal microscope (Leica microsystems, Germany) using a 93x glycerin objective (NA = 1.3, WD = 0.30 mm, HC PL APO motCORR STED white). Images displayed in the figure are presented as a maximum projection of 4 z-stack images.

Warfarin treatment studies

12 week-old female C57BL/6 mice (UT Southwestern breeding core) were administered 1mg/L warfarin (Coumadin, Bristol-Myers Squibb Company) in drinking water. After five months of treatment mice were sacrificed and the mammary glands were dissected, fixed in 2% paraformaldehyde in PBS, stained with Carmine alum solution (Sigma C1022), cleared in xylene, mounted with Organo/Limonene (Sigma O8015) and imaged using brightfield tile scan with a Nikon TE2000. Treatment of pre-pubescent mice were initiated in 3 week old mice post-weaning. Mice were treated with either pure water or warfarin (1 mg/L) containing drinking water for 5 weeks prior to harvest of mammary glands and carmine alum staining as described above.

Generation of *MMTV-Wnt1:AXL+/+* and *MMTV-Wnt1:AXL*$^{LacZ/LacZ}$ transgenic animals

MMTV-Wnt1 male mice (Jackson Laboratory) (Donehower et al., 1995; Tsukamoto et al., 1988) (kindly provided by Prof. Stein Ove Døskeland) were crossed with females of the *AXLLacZ* knock-in strain (B6.129P2-*AXL*^{tm1Dgen}, figure S5) to generate *MMTV-Wnt1*-positive females that develop spontaneous mammary tumors in a wildtype AXL$^{+/+}$ (*MMTV-Wnt1:AXL+/+)* and *AXL*-null (*MMTV-Wnt1:AXL*$^{LacZ/LacZ}$) background. Tumor formation was monitored by weekly palpation of the mammary glands from 1 month to 14 months of age. Previous studies showed that all *MMTV-Wnt1* females developed tumors within 1 year (Donehower et al., 1995, Tsukamoto et al., 1988). Mice that did not develop tumors within the duration of the 14-month observation period were scored as tumor-free.

Mammary tumor incidence studies

Female NOD/SCID *b2mnull* and Balb/c mice (6–8 weeks old; Gades Institute, University of Bergen) were used for tumor studies. The orthotopic 4T1-GFP-Luc mouse mammary carcinoma model was conducted as previously described (Gjerdrum et al., 2010). Cells were suspended in MEM/ EBSS medium/Matrigel (1: 1) (1x 10^6 cells in 50 µl) and were subsequently injected into the mammary fat pad of female BALB/c mice. Tumor growth were monitored and imaging of the ventral view were performed by the eXplore Optix Imaging System 10–15 min after D-luciferin (Biosynth) injection.

Xenograft tumor-initiation studies

Xenograft tumor-initiation studies were conducted as described by (Gupta et al., 2009). HMLER cells stably transduced by retroviral vectors (Slug, shLuc, shAXL) were suspended in DMEM/Matrigel (1:1) in a total volume of 50 µl and injected subcutaneously into the flank of NOD-SCID mice. Tumor incidence was monitored for up to 60 days after injection. For syngeneic tumor seeding studies, 4T1 cells were pretreated for 4 days with paclitaxel (3 nM) and bemcentinib (600 nM), and allowed to recover in the absence of drug for 1 week prior to injection. Tumor formation was assayed by palpation and caliper measurement between 7-9 days post implantation.

Histology and morphometry

The ductal morphology of mammary glands from 16 week old nulliparous *Axl*$^{+/+}$ and*: Axl*$^{LacZ/LacZ}$ of the B6.129P2-AXLtm1Dgen strain (The Jackson Laboratory, Bar Harbour, ME) mice were examined by hematoxylin/eosin (HE) stained FFPE tissue sections and carmine alum stained whole-mount specimens. Quantification of ductal area (µm2) per epithelial structure were performed on HE stained FFPE sections from *Axl*$^{+/+}$ (n= 7) and *Axl*$^{LacZ/LacZ}$ (n= 9) animals. Images were obtained using the NikonTE2000 microscope and area (µm2/ structure) were recorded using the Nikon software from 10 separate fields/ gland (Mann-Whitney p< 0.0001). Carmine alum stained mammary gland whole-mounts of 16-week old nulliparous *Axl*$^{+/+}$ (n= 8) and *Axl*$^{LacZ/LacZ}$ (n= 9) (B6.129P2-AXLtm1Dgen Strain, The Jackson Laboratory) mice were prepared and imaged as described. Both inguinal glands were included in the analysis. Ducts were partitioned from the background using image thresholding with MATLAB. The binary image obtained was sliced vertically pixel-wise. Segment lengths from the same duct were measured and averaged. FFPE sections from the mouse mammary fat pad tissue were stained by IHC-P for detection of ERalpha (ESR1) (ab37453, Abcam), Progesterone receptor (ab2765), and Ki67 (ab15580, Abcam). DAKO EnVisionTM System-HRP (DAB) for Rabbit primary antibodies (K4011, DAKO) were applied according to the manufacturer's instructions. Antibodies were diluted in antibody-diluent with

background reducing components (S3022, DAKO). Stained sections were counterstained with haematoxylin, prior to mounting using Faramount Aqueous Mounting Medium (S3225, DAKO). FFPE sections from the mouse mammary fat pad tissue were assessed for progesterone and estrogen receptor expression (scored strong or weak versus negative by trained pathologists), and proliferation rate by Ki-67 expression in luminal cells in the glands and duct structures. We used 25 high-power fields (x 400) and counted 20 luminal cells in each field (total of 500 luminal cells per case). Cells with cytoplasmic staining were not considered positive, and myoepithelial cells were not evaluated. All intensities of nuclear positivity were recorded as positive. The percentage of positive cells in each case was then calculated.

Statistical analysis

Where not otherwise stated, Graphpad Prism 5.0 for PC and Graphpad Prism 6.0 for Mac and MATLAB were used for statistical analysis using tests specified in the Figure Legends. The following symbols are shown to report established statistical significance: NS = $P > 0.05$, *$P \le 0.05$, **$P \le 0.01$, ***$P \le 0.001$, ****$P \le 0.0001$.

Supplemental references

AMIR EL, A. D., DAVIS, K. L., TADMOR, M. D., SIMONDS, E. F., LEVINE, J. H., BENDALL, S. C., SHENFELD, D. K., KRISHNASWAMY, S., NOLAN, G. P. & PE'ER, D. 2013. viSNE enables visualization of high dimensional single-cell data and reveals phenotypic heterogeneity of leukemia. *Nat Biotechnol,* 31**,** 545-52.

BODENMILLER, B., ZUNDER, E. R., FINCK, R., CHEN, T. J., SAVIG, E. S., BRUGGNER, R. V., SIMONDS, E. F., BENDALL, S. C., SACHS, K., KRUTZIK, P. O. & NOLAN, G. P. 2012. Multiplexed mass cytometry profiling of cellular states perturbed by small-molecule regulators. *Nat Biotechnol,* 30**,** 858-67.

CURTIS, C., SHAH, S. P., CHIN, S. F., TURASHVILI, G., RUEDA, O. M., DUNNING, M. J., SPEED, D., LYNCH, A. G., SAMARAJIWA, S., YUAN, Y., GRAF, S., HA, G., HAFFARI, G., BASHASHATI, A., RUSSELL, R., MCKINNEY, S., GROUP, M., LANGEROD, A., GREEN, A., PROVENZANO, E., WISHART, G., PINDER, S., WATSON, P., MARKOWETZ, F., MURPHY, L., ELLIS, I., PURUSHOTHAM, A., BORRESEN-DALE, A. L., BRENTON, J. D., TAVARE, S., CALDAS, C. & APARICIO, S. 2012. The genomic and transcriptomic architecture of 2,000 breast tumours reveals novel subgroups. *Nature,* 486**,** 346-52.

DONEHOWER, L. A., GODLEY, L. A., ALDAZ, C. M., PYLE, R., SHI, Y. P., PINKEL, D., GRAY, J., BRADLEY, A., MEDINA, D. & VARMUS, H. E. 1995. Deficiency of p53 accelerates mammary tumorigenesis in Wnt-1 transgenic mice and promotes chromosomal instability. *Genes Dev,* 9**,** 882-95.

DONTU, G., ABDALLAH, W. M., FOLEY, J. M., JACKSON, K. W., CLARKE, M. F., KAWAMURA, M. J. & WICHA, M. S. 2003. In vitro propagation and transcriptional profiling of human mammary stem/progenitor cells. *Genes Dev,* 17**,** 1253-70.

FELLENBERG, K., HAUSER, N. C., BRORS, B., NEUTZNER, A., HOHEISEL, J. D. & VINGRON, M. 2001. Correspondence analysis applied to microarray data. *Proc Natl Acad Sci U S A,* 98**,** 10781-6.

GJERDRUM, C., TIRON, C., HOIBY, T., STEFANSSON, I., HAUGEN, H., SANDAL, T., COLLETT, K., LI, S., MCCORMACK, E., GJERTSEN, B. T., MICKLEM, D. R., AKSLEN, L. A., GLACKIN, C. & LORENS, J. B. 2010. Axl is an essential epithelial-to-mesenchymal transition-induced regulator of breast cancer metastasis and patient survival. *Proc Natl Acad Sci U S A,* 107**,** 1124-9.

GUPTA, P. B., ONDER, T. T., JIANG, G., TAO, K., KUPERWASSER, C., WEINBERG, R. A. & LANDER, E. S. 2009. Identification of selective inhibitors of cancer stem cells by high-throughput screening. *Cell,* 138**,** 645-59.

HU, Y. & SMYTH, G. K. 2009. ELDA: extreme limiting dilution analysis for comparing depleted and enriched populations in stem cell and other assays. *J Immunol Methods,* 347**,** 70-8.

LABARGE, M. A., GARBE, J. C. & STAMPFER, M. R. 2013. Processing of human reduction mammoplasty and mastectomy tissues for cell culture. *J Vis Exp.*

LIM, E., VAILLANT, F., WU, D., FORREST, N. C., PAL, B., HART, A. H., ASSELIN-LABAT, M. L., GYORKI, D. E., WARD, T., PARTANEN, A., FELEPPA, F., HUSCHTSCHA, L. I., THORNE, H. J., FOX, S. B., YAN, M., FRENCH, J. D., BROWN, M. A., SMYTH, G. K., VISVADER, J. E. & LINDEMAN, G. J. 2009. Aberrant luminal progenitors as the candidate target population for basal tumor development in BRCA1 mutation carriers. *Nat Med,* 15**,** 907-13.

PELISSIER VATTER, F. A., SCHAPIRO, D., CHANG, H., BOROWSKY, A. D., LEE, J. K., PARVIN, B., STAMPFER, M. R., LABARGE, M. A., BODENMILLER, B. & LORENS, J. B. 2018. High-Dimensional Phenotyping Identifies Age-Emergent Cells in Human Mammary Epithelia. *Cell Rep,* 23**,** 1205-1219.

SUBRAMANIAN, A., TAMAYO, P., MOOTHA, V. K., MUKHERJEE, S., EBERT, B. L., GILLETTE, M. A., PAULOVICH, A., POMEROY, S. L., GOLUB, T. R., LANDER, E. S. & MESIROV, J. P. 2005. Gene set enrichment analysis: a knowledge-based approach for interpreting genome-wide expression profiles. *Proc Natl Acad Sci U S A,* 102**,** 15545-50.

SWIFT, S., LORENS, J., ACHACOSO, P. & NOLAN, G. P. 2001. Rapid production of retroviruses for efficient gene delivery to mammalian cells using 293T cell-based systems. *Curr Protoc Immunol,* Chapter 10**,** Unit 10 17C.

TAN, T. Z., MIOW, Q. H., MIKI, Y., NODA, T., MORI, S., HUANG, R. Y. & THIERY, J. P. 2014. Epithelial-mesenchymal transition spectrum quantification and its efficacy in deciphering survival and drug responses of cancer patients. *EMBO Mol Med,* 6**,** 1279-93.

TSUKAMOTO, A. S., GROSSCHEDL, R., GUZMAN, R. C., PARSLOW, T. & VARMUS, H. E. 1988. Expression of the int-1 gene in transgenic mice is associated with mammary gland hyperplasia and adenocarcinomas in male and female mice. *Cell,* 55**,** 619-25.

ZIVANOVIC, N., JACOBS, A. & BODENMILLER, B. 2014. A practical guide to multiplexed mass cytometry. *Curr Top Microbiol Immunol,* 377**,** 95-109.